

Core-corona separation in the UrQMD hybrid modelJ. Steinheimer^{1,2} and M. Bleicher^{1,2}¹*Institut für Theoretische Physik, Goethe-Universität, Max-von-Laue-Strasse 1, D-60438 Frankfurt am Main, Germany*²*Frankfurt Institute for Advanced Studies (FIAS), Ruth-Moufang-Strasse 1, D-60438 Frankfurt am Main, Germany*

(Received 26 April 2011; published 9 August 2011)

We employ the UrQMD transport + hydrodynamics hybrid model to estimate the effects of a separation of the hot equilibrated core and the dilute corona created in high-energy heavy-ion collisions. It is shown that the fraction of the system that can be regarded as an equilibrated fireball changes over a wide range of energies. This has an impact, especially on strange particle abundances. We show that such a core corona separation allows for an improvement in the description of strange particle ratios and flow as a function of beam energy as well as strange particle yields as a function of centrality.

DOI: [10.1103/PhysRevC.84.024905](https://doi.org/10.1103/PhysRevC.84.024905)

PACS number(s): 25.75.Ag, 24.10.Nz, 24.10.Lx

I. INTRODUCTION

The objective of the low-energy heavy-ion collider programs at the Relativistic Heavy Ion Collider (RHIC) facility at Brookhaven National Laboratory (BNL) the Super Proton Synchrotron (SPS) at the European Organization for Nuclear Research (CERN) and the planned projects at the Nuclotron-based Ion Collider (NICA) in Dubna and the Facility for Antiproton and Ion Research (FAIR) near the Gesellschaft für Schwerionenforschung (GSI) facility is to find evidence for the onset of a deconfined phase [1,2]. At the highest RHIC energies, experiments [3–6] have already confirmed a collective behavior of the created (partonic) system, signaling a change in the fundamental degrees of freedom. Lattice quantum chromodynamics (QCD) calculations indeed expect a deconfinement crossover to occur in systems created at the RHIC. As theoretical predictions on the thermodynamics of finite density QCD are quite ambiguous [7–14], one would hope to confirm experimentally a possible first-order phase transition, and consequently the existence of a critical end point, by mapping out the phase diagram of QCD in small steps.

Hadronic bulk observables, which are usually connected to the onset of deconfinement, are the particle flow and its anisotropies as well as particle yields and ratios [15–30]. It has often been proposed that, e.g., the equilibration of strangeness would be an indication of the onset of a deconfined phase, although this idea is still under heavy debate [31–34].

The interpretation of experimental results and their relation to the deconfinement phase transition is most often circumstantial, and extensive model studies are required to understand the multitude of observables. Therefore, dynamical models for the description of relativistic heavy-ion collisions are needed as input for the interpretation of the observed phenomena.

Dynamical approaches to heavy-ion collisions are often based on two complementary theoretical concepts, the first being relativistic fluid dynamics [35–44]. In this approach, one assumes that the produced system can be described as an expanding liquid that is in local thermal equilibrium. The assumption of local equilibration is usually disputed, which led to the development of hydrodynamic models that employ viscous corrections. Apart from these complications,

a general advantage of the hydrodynamic approach is that an equation of state, which contains the information on the active degrees of freedom of the system (potentially including a phase transition), can be easily introduced in the model.

The second type of model is based on the relativistic Boltzmann transport equation [45–51]. The applicability of this equation is independent of any equilibrium assumption, which makes it superior to the hydrodynamic approach in this respect. However, the implementation of a phase transition in such a microscopic model is far more complicated and still poses a great challenge to theorists.

To obtain a more comprehensive picture of the whole dynamics of heavy-ion reactions, various so called micro+macro hybrid approaches have been developed during the past few years [52] to combine the benefits of the two mutually complementary approaches discussed earlier. Here, one employs initial conditions that are calculated from a nonequilibrium model followed by an ideal or viscous hydrodynamic evolution coupled to the Boltzmann equation for the final state [44,53–62].

In this paper, we present a study of the effects of the assumption of local thermal and chemical equilibrium in the description of heavy-ion collisions at different beam energies. In particular, we want to discuss cases in which only parts of a created fireball can be regarded as being equilibrated. Following previous explorations, such a system can be divided into a hot and dense core and a dilute corona [63,64], where each part of the system should be treated on a different theoretical footing. We will apply the UrQMD transport/hydrodynamics hybrid model as described in [65] and modify it to allow for a consistent simultaneous description of a core-corona separated system. Let us remark that the present model allows us only to study the effects of local thermal and chemical equilibration, while it does not allow us to pin down the actual dynamical processes that induce the early equilibration. In fact, the processes responsible for fast equilibration of the produced matter (probably instabilities or multiparticle interactions [34,66]) still pose a great theoretical challenge in modeling heavy-ion collisions.

In the following, we will first explain briefly the concept and implementation of the UrQMD hybrid model and how it is extended to allow for a consistent separation of the dense core and dilute corona of the fireball that is obtained. Then we present results that are sensitive to such a separation and discuss them in order before making concluding remarks.

II. THE HYBRID MODEL

Hybrid approaches to unite hydrodynamics and transport equations were proposed 10 years ago [60,62] and have since been employed for a wide variety of investigations [56,57,67,68]. The hybrid approach presented here is based on the integration of a hydrodynamic evolution into the UrQMD transport model [65,69,70]. During the first phase of the evolution, the particles are described by UrQMD as a string/hadronic cascade. Once the two colliding nuclei have passed through each other, the hydrodynamic evolution starts at the time $t_{\text{start}} = 2R/\sqrt{\gamma_{\text{c.m.}}^2 - 1}$, where $\gamma_{\text{c.m.}}$ denotes the Lorentz gamma of the colliding nuclei in their center-of-mass frame. While the spectators continue to propagate in the cascade, all other particles, i.e., their baryon charge densities and energy-momentum densities, are mapped to the hydrodynamic grid. By doing so, one explicitly forces the system into a local thermal equilibrium for each cell. In the hydrodynamic part, we solve the conservation equations for energy and momentum as well as the net baryon number current, while for the net strange number we assume it to be conserved and equal to zero locally. Solving only the equations for the net baryon number is commonly accepted in hydrodynamic models, although we have shown in earlier [71] publications that net strangeness may fluctuate locally. The implementation of an explicit propagation for the net strange density is planned for the future. Such an extension of the model will also require that the equation of state be extended in the net strange sector, which is an investigation that is currently underway and will be addressed in future publications.

The hydrodynamic evolution is performed using the SHASTA algorithm [38] with an equation of state that incorporates a chiral as well as a deconfinement crossover and which is in agreement with thermodynamic results from lattice calculations [72]. At the end of the hydrodynamic phase, the fields are mapped to particle degrees of freedom using the Cooper-Frye equation [73]. The transition from the hydrodynamic prescription to the transport simulation is done gradually in transverse slices of thickness 0.2 fm once all cells in a given slice have an energy density lower than five times the ground-state energy density (see also [74]). The temperature at $\mu_B = 0$, which corresponds to such a switching density, is roughly $T = 170$ MeV, which is close to what is expected to be the critical temperature. Detailed information of the transition curve in the phase diagram can be found in [69]. After this, the final-state interactions and decays of the particles are calculated and the system freezes out dynamically within the UrQMD framework.

For an extensive description of the model, the reader is referred to [69,74].

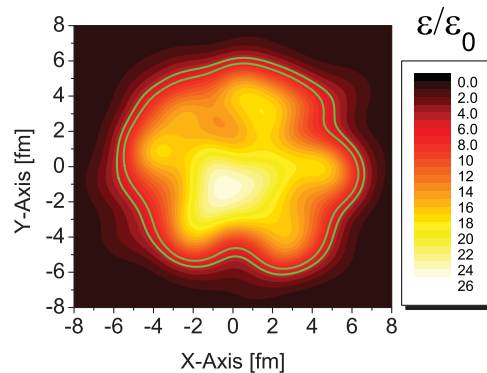


FIG. 1. (Color online) Contour plot of the local rest frame energy density in the transverse plane ($z = 0$) of a central ($b = 0$) collision of Pb + Pb at $E_{\text{lab}} = 40A$ GeV. The energy density is normalized to the ground-state energy density ($\epsilon_0 \approx 145$ MeV/fm³). The two green lines correspond to lines of a constant energy density of $\epsilon/\epsilon_0 = 5$ and 7.

III. SEPARATING CORE AND CORONA

Essentially all previous hybrid model calculations have assumed that the whole system created enters a phase of local thermal equilibrium. As the local rest frame energy density varies in coordinate space, one would expect that some portions of the created system, already in the beginning of the evolution, have densities that are smaller than the transition energy density. When performing hydrodynamic simulations, one generally neglects such portions of the system that never really enter an equilibrated phase. As a first step, we want to estimate quantitatively how good such an assumption is. As a visualization of the problem, Figs. 1 and 2 show contour plots of the local rest frame energy densities (normalized to the ground-state energy density) in the transverse plane ($z = 0$) of central Pb + Pb collisions at two different energies. Figure 1 depicts the distribution for $E_{\text{lab}} = 40A$ GeV and Fig. 2 for $E_{\text{lab}} = 160A$ GeV. One can clearly see that the energy densities reached in the center of the system exceed the transition criterion for both cases, while the energy density

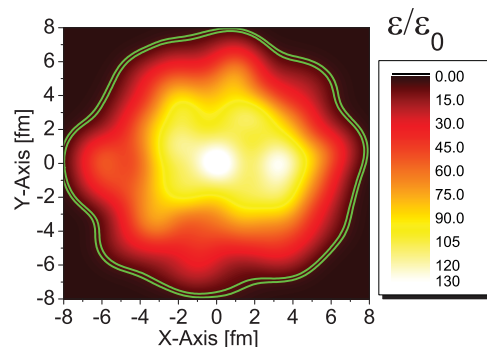


FIG. 2. (Color online) Contour plot of the local rest frame energy density in the transverse plane ($z = 0$) of a central ($b = 0$) collision of Pb + Pb at $E_{\text{lab}} = 160A$ GeV. The energy density is normalized to the ground-state energy density ($\epsilon_0 \approx 145$ MeV/fm³). The two green lines correspond to lines of a constant energy density of $\epsilon/\epsilon_0 = 5$ and 7.

for $E_{\text{lab}} = 160A$ GeV is roughly five times that for $E_{\text{lab}} = 40A$ GeV. The green solid lines are lines of constant energy density, $\epsilon = 5$ and 7 times ϵ_0 . For the higher beam energy, almost the entire system seems to have an energy density larger than this criterion, while for $E_{\text{lab}} = 40A$ GeV this is not the case. One observes that parts of the system lie already outside of the hot and dense region.

In the following, we describe how one can separate the system that is produced in the heavy-ion collision in a dense core part, which will be propagated using the hydrodynamic prescription, and a dilute corona part, for which we assume the UrQMD transport approach to be the correct model.

The idea that the fireball created in a heavy-ion collision can be divided into a dense core that expands collectively and a dilute corona that is dominated by hadronic scatterings is not new. The first time this idea was adapted in a dynamical model for heavy-ion collisions was in [63]. In that approach, the system was divided into transverse cells of a certain pseudorapidity range. Whenever the transverse string density in such a cell was above a certain value, it was considered to be part of the equilibrated core. Otherwise, it was considered to be part of the corona. In a different approach, the core-corona separation was made using a Monte Carlo–Glauber model and distinguishing between nucleons that have interacted more than once with those that have interacted only once, which were regarded as part of the corona [75–78].

For the present study, we will apply a method similar to that used in [63]. At the time t_{start} of the transition from the UrQMD model to the hydrodynamic phase, we calculate the scalar constituent quark number density (mesons count 2 for $q + \bar{q}$ and baryons count 3 for $q + q + q$) at the position of every particle. This is done by describing every hadron as a Lorentz contracted Gaussian distribution of its constituent quark number and then summing over the contributions of all particles to a given space point. As a result, one obtains the quark number density ρ_q at the position of every hadron in the UrQMD model. If the density at the particle position is above a certain critical separation density, it is used to calculate the initial density profiles for the hydrodynamic evolution as outlined above. If the density is below the separating density, it will remain in the transport model and will be propagated there in parallel to the hydrodynamic evolution. After the transition from the hydrodynamic phase back to the transport model occurs, all particles can then interact again and decouple dynamically. Note that this procedure is similar to the one applied in [63], although a distinct difference is that we calculate the scalar density at every particle’s position in coordinate space. As for higher energies, the particle density should be roughly independent of the pseudorapidity (boost invariance). The definition of a corona via the transverse string density as in [63] is sufficient. For lower energies, this relation does not hold anymore and the full calculation of the particle number density seems more appropriate. On the other hand, the present approach becomes unfeasible at some point as particles from all rapidities contribute to the local density of any other particle. One could, therefore, apply a cut in pseudorapidity (of $\Delta\eta = 0.5$) for particles that contribute to the local density $\rho_q(\vec{x})$.

Our procedure introduces the density ρ_q as another parameter in the model. In the present investigation, we will

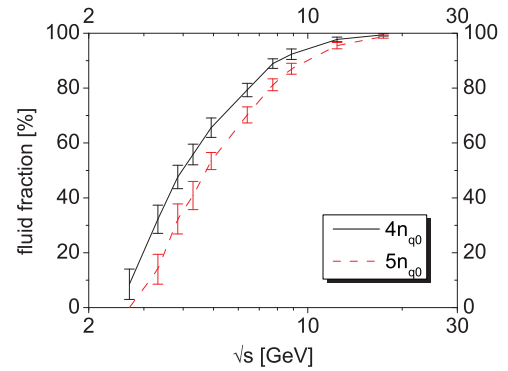


FIG. 3. (Color online) Fraction of the total energy of the system, which is transferred into the hydrodynamic phase as a function of the center-of-mass beam energy, for central ($b < 3.4$ fm) collisions of AuAu/PbPb. The black line corresponds to a cut of energy density of $\rho_q = 4\rho_{q0}$ and the red dashed line to $\rho_q = 5\rho_{q0}$. The error bars indicate the mean deviation of the fluid fraction on an event-by-event basis.

constrain this parameter to lie between four and five times ρ_{q0} (where $\rho_{q0} = 0.15 \times 3 \text{ fm}^{-3}$, the ground-state quark density at $T = 0$). This choice of parameter is taken because we try to keep the cutoff density from entering the hydrodynamic phase close to the density criterion for the transition from the hydrodynamic phase back to the hadronic afterburner. The values of four and five times ρ_{q0} closely correspond to the energy densities of five and seven times ϵ_0 when we consider a hadron resonance gas, which includes the same degrees of freedom as does UrQMD.

IV. ENERGY DEPENDENCE

In this section, we will concentrate in the beam energy dependence of the effects of a core-corona separation as described above. We will apply the model for most central ($b < 3.4$ fm) collisions of AuAu/PbPb at different beam energies and present the results for choices of the density cutoff parameter of four and five times ρ_{q0} .

Figure 3 shows the fraction of the total energy of the colliding system (excluding spectators), which is transferred into the hydrodynamic phase. For the lowest beam energy, $E_{\text{lab}} = 2A$ GeV, only a vanishing fraction of the system can be regarded as being in local thermal equilibrium. The fraction increases slowly with the beam energy, while only at the highest Super Proton Synchrotron (SPS) energies can one regard the whole system as being equilibrated. Changing the density cutoff parameter ρ_q only results in a small shift at intermediate beam energies, while at the highest SPS energies the density gradients of the produced system are so large that the result is insensitive to the exact value of the ρ_q parameter. The “error” bars in the figure represent the mean deviation of the fluid fraction on an event-by-event basis.

As a next step, we investigate the dependence of experimental hadronic observables, such as the particle yields and flow, on the separation procedure. Figure 4 depicts the beam energy dependence of the ratios of protons to pions (upper plot) and positively charged kaons and pions (lower plot) in

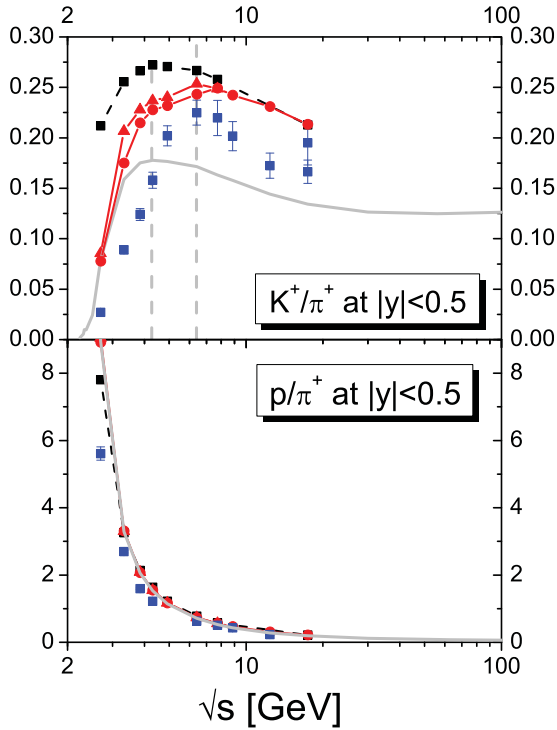


FIG. 4. (Color online) Particle ratios of protons to pions, upper plot, and positively charged kaons to pions, lower plot. The results are for the midrapidity region ($|y| < 0.5$) of central ($b < 3.4$ fm) collisions of AuAu/PbPb ions. The different model results (lines are explained in the text) are compared to experimental data. The horizontal dashed lines are shown to point out the peak positions of the K^+/π^+ ratio for the standard UrQMD calculation and the data.

the midrapidity region of central $b < 3.4$ heavy-ion collisions ($|y| < 0.5$). Here, as well as in the following plots, for comparison the solid gray line represents the results of the default UrQMD calculation without an intermediate hydrodynamic stage. The black dashed line with square symbols depicts the hybrid model results without any core-corona separation, which means that the whole fireball is regarded as being in local thermodynamic equilibrium. The red solid lines show the results obtained when we apply our core-corona separation using the two different values of the density cutoff parameter (triangles: $\rho_q = 4\rho_{q0}$, circles: $\rho_q = 5\rho_{q0}$). The model results are compared to data from different experiments [79–86], which are shown as blue square symbols.

For the nonstrange protons and pions, the assumption of local thermal equilibration seems not to change the results on the particle ratio, and the different model calculations give a rather good description of the data.

However, if one looks at the ratio of the positively charged kaons to pions, we observe considerable differences in the results obtained from the different approaches. Generally, the assumption of thermal equilibrium drastically enhances the production of strange particles when compared to the UrQMD nonequilibrium approach. In particular, for the very low beam energies, this leads to a drastic overestimation of the ratios involving strange particles in the standard UrQMD hybrid model. In contrast, using the core-corona

separation approach, the fraction of the system for which local equilibrium is assumed changes with the beam energy. Therefore, for the lowest energies, one smoothly recovers the default UrQMD results. At intermediate energies, the core-corona result is generally in between the transport model and the default hybrid model. It should be noted that the position of the peak in the K^+/π^+ ratio depends on the core fraction and only coincides with the available data for the new core-corona approach. For the default hybrid and transport model calculations, the peak appears at lower energies. As a side remark, let us state that in the usual transport simulations, the position of the peak is solely determined by the transition from a baryon- to a meson-dominated system, while for the present core-corona approach the slow onset of strangeness equilibration plays the driving role.

The beam energy dependence of strange baryon to pion ratios is shown in Fig. 5, where the vertical dashed lines again indicate the positions of the peaks in the K^+/π^+ ratio. The description of the Λ/π is again improved when one assumes that only a part of the system is fully equilibrated. For the Ξ^-/π ratio (lower plot in Fig. 5), the default UrQMD calculation drastically underpredicts the production rate of the multistrange baryon. Even the default hybrid model result seems to underestimate the data slightly, and this ratio even decreases in our new core-corona approach. However, the effect is smaller than for the single strange hadrons. For

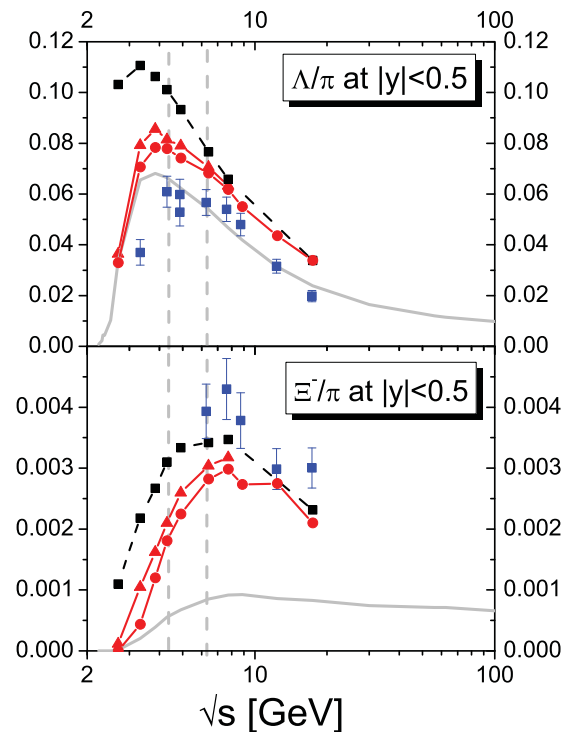


FIG. 5. (Color online) Particle ratios of Λ 's to pions, upper plot, and negatively charged Ξ 's to pions, lower plot. The results are for the midrapidity region ($|y| < 0.5$) of central ($b < 3.4$ fm) collisions of AuAu/PbPb ions. The different model results (lines are explained in the text) are compared to experimental data. The horizontal dashed lines are shown to point out the peak positions of the K^+/π^+ ratio for the standard UrQMD calculation and the data.

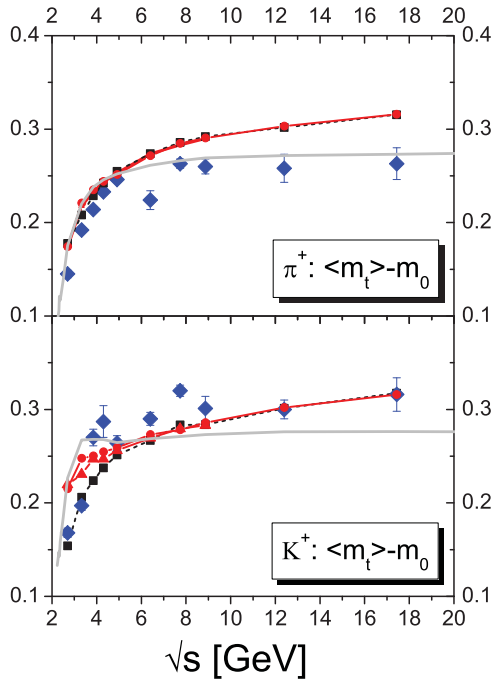


FIG. 6. (Color online) Excitation functions of the mean transverse mass, for the midrapidity region ($|\eta| < 0.5$) of central ($b < 3.4$ fm) collisions of AuAu/PbPb ions. Positively charged pions are shown in the upper panel and kaons in the lower panel. Experimental data are shown as diamond symbols [80,81,85] (lines are explained in the text).

both strange baryon ratios, the peak position is found to be independent of the applied model parametrization.

Next we turn to the investigation of average particle flow. Even more than particle yields, their momenta and collective motion could depend on the degree of equilibration in the system. Figure 6 shows the excitation functions of the mean transverse masses of pions and kaons compared to data [80,81,85]. For the positively charged pions, we observe almost no dependence on the parametrization of the core-corona separation in the hybrid model. The K^+ excitation

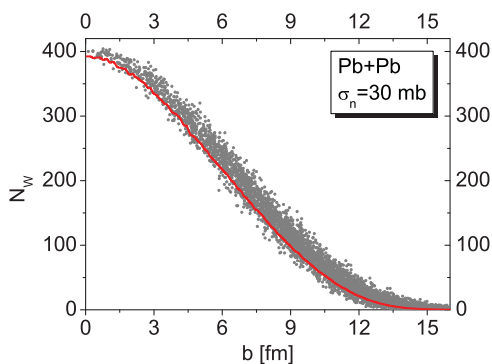


FIG. 7. (Color online) The dependence of the number of wounded nucleons N_w as a function of the impact parameter for collisions of heavy ions at $E_{\text{lab}} = 40A$ GeV. The red line shows the result from a Monte Carlo-Glauber simulation, assuming an inelastic nucleon-nucleon cross section of $\sigma_n = 30$ mb. The points depict the results from the hybrid model calculation on an event-by-event basis.

function (shown in the lower part of Fig. 6) shows small differences at low beam energies. Here the mean transverse mass is increased in the nonequilibrium transport approach as compared to the hybrid model calculation. Interestingly, the description of the π^+ data at high energies is better in the default UrQMD approach, while for the K^+ it is better in the hybrid model.

In [87] it was pointed out that the surplus of low momentum pions in the data as compared to the hybrid model calculations, which would lead to a decrease in the K^+/π^+ and the mean m_T of pions, can contribute to heavy resonance contributions as well as nonequilibrium corrections to the hydrodynamic phase.

V. CENTRALITY DEPENDENCE

Instead of varying the temperature and density by a beam energy scan, such a variation could also be achieved by changing the centrality of the collision. In our calculation, this can be done by changing the impact parameter b . In experiment, as the determination of the impact parameter is usually not straightforward, one usually gives observables as a function of the number of wounded nucleons. This is the number of nucleons that have undergone a primary binary collision, and their energy can therefore contribute to the total energy of the fireball.

In the transport and hybrid model calculations, the definition of the number of wounded nucleons is by no means trivial. Late-time secondary interactions, which would only excite the spectator fragment, can remove spectator nucleons from the fragment, leading to an overestimation of N_w . We therefore define the number of wounded nucleons in our model calculations as the number of nucleons that have not interacted until the time t_{start} (see the definition above). In

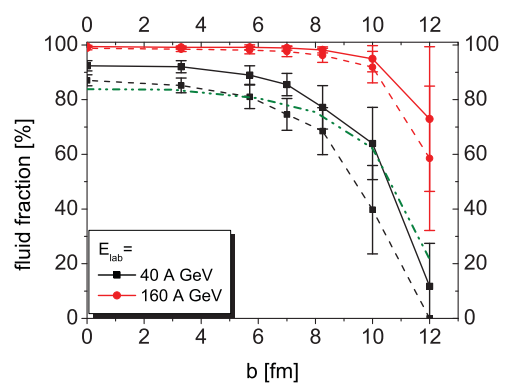


FIG. 8. (Color online) Fraction of the total energy of the system, which is transferred into the hydrodynamic phase as a function of the impact parameter b , for collisions of Pb nuclei. The red lines with circles depict the results for $E_{\text{lab}} = 40A$ GeV and the black lines with squares for $E_{\text{lab}} = 160A$ GeV. We compare results for both choices of the core density parameter $\rho_q = 4$ (solid lines) and $5\rho_{q0}$ (dashed lines). If a cut in pseudorapidity is applied for the calculations at $E_{\text{lab}} = 160A$ GeV, we obtain the green dash-dotted line as a result for $\rho_q = 5\rho_{q0}$. The error bars indicate the mean deviation of the fluid fraction on an event-by-event basis.

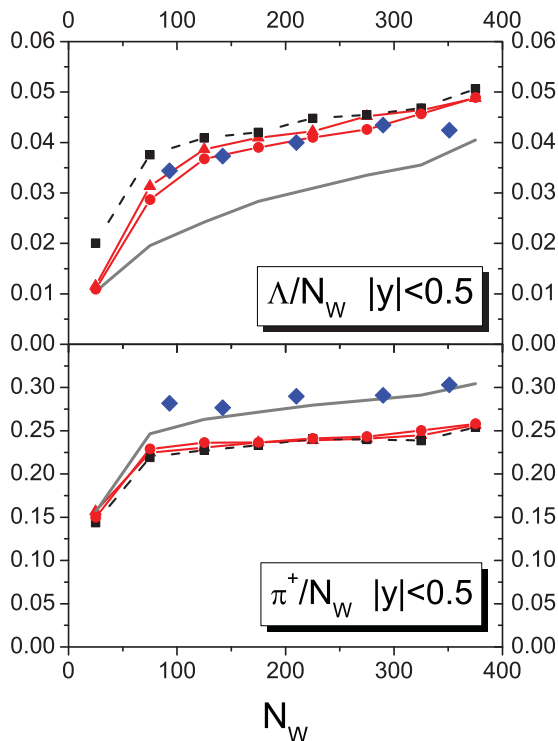


FIG. 9. (Color online) Centrality dependence of the number of Λ 's (upper plot) and pions (lower plot) per wounded nucleon, produced in heavy-ion collisions at $E_{\text{lab}} = 40A$ GeV, compared to data. Shown is the yield at midrapidity $|y| < 0.5$. The gray line is the result from the default UrQMD model and the dashed black line with squares depicts the default hybrid model results. The solid red lines show the calculations with the core-corona separated hybrid model with two different values of the core density parameter $\rho_q = 4$ (triangles) and $5\rho_{q0}$ (circles).

this way, one obtains a dependence of N_W on the impact parameter b , which is in agreement with the estimate of a Monte Carlo–Glauber model calculation [88,89] (see Fig. 7). Such a Glauber model is often used to estimate N_W from experimental data. Therefore, we can compare our results with experiment using our definition of N_W without invoking the real experimental trigger conditions.

Let us start with an investigation of the fluid fraction as a function of the impact parameter. Figure 8 displays the fluid fraction for two different energies as a function of the impact parameter b . For each energy, the results are shown for the two different cutoff densities, where the solid lines correspond to $\rho_q = 5\rho_{q0}$ and the dashed lines to $\rho_q = 4\rho_{q0}$. The green dash-dotted line shows the effect of the cut in pseudorapidity in the definition of the density for $E_{\text{lab}} = 160A$ GeV.

For both energies, one observes a dependence of the fluid fraction on the input parameter. While at $E_{\text{lab}} = 40A$ GeV (red lines with circles) this dependence is rather strong, it is rather weak for $E_{\text{lab}} = 160A$ GeV (black lines with squares). If a cut in η for the calculation of the local density is applied, the impact parameter dependence becomes much stronger for the highest SPS energy (green dash-dotted line).

In the last part of this paper, we will discuss the results on the centrality dependence of different hadronic observables and

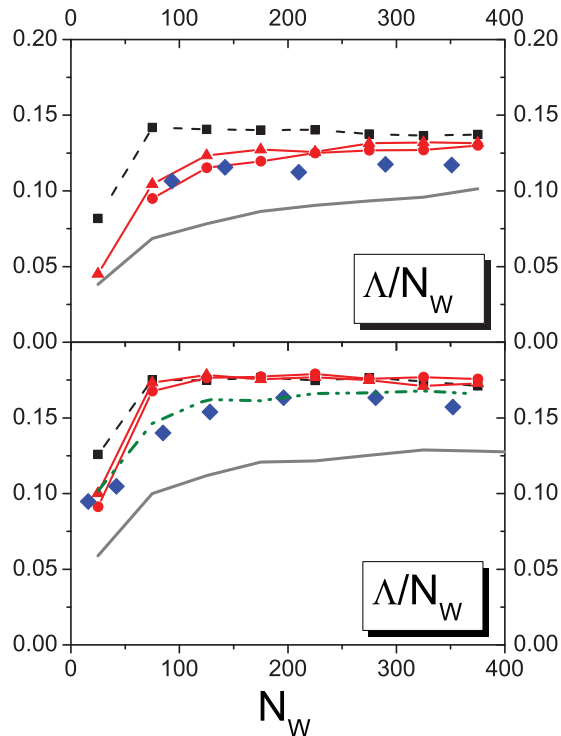


FIG. 10. (Color online) Centrality dependence of the number of Λ 's per wounded nucleon produced in heavy-ion collisions at $E_{\text{lab}} = 40A$ GeV (upper plot) and $160A$ GeV (lower plot), compared to data. Shown is the 4π integrated yield. The line styles are as in the previous figure. If a cut in pseudorapidity is applied for the calculations at $E_{\text{lab}} = 160A$ GeV, we obtain the green dash-dotted line as a result for $\rho_q = 5\rho_{q0}$.

compare them to data [79,90–93] (the centrality selection with regard to the number of wounded nucleons is taken from [94]). Figure 9 displays the midrapidity ($|y| < 0.5$) yields of pions and Λ 's divided by the number of wounded nucleons as a function of N_W . Here the analysis is restricted to results for $E_{\text{lab}} = 40A$ GeV due to the stronger dependence of the fluid fraction on the centrality at this energy. The different lines depict the results for the default UrQMD model in its cascade mode (gray line), the default hybrid model (black dashed line with square symbols), and the different parametrizations of the core-corona separated hybrid model (red lines with symbols). For the most central collisions, all models reproduce the data equally well, while the centrality dependence can only be captured by the hybrid model, and especially the core-corona separated versions.

The pion yield, on the other hand, shows only a weak sensitivity to the presence of a corona and is well reproduced with the UrQMD cascade version.

While Fig. 9 only displays the results at $E_{\text{lab}} = 40A$ GeV, Fig. 10 shows a comparison of the centrality dependence of the Λ multiplicity for $E_{\text{lab}} = 40$ and $160A$ GeV. For the lower energy, the core-corona separated version again gives the best result. While at the highest SPS energy, all hybrid model results show almost no centrality dependence, which is in contrast to experimental data, it seems that our definition of the corona begins to fail when the beam energy becomes so large that the

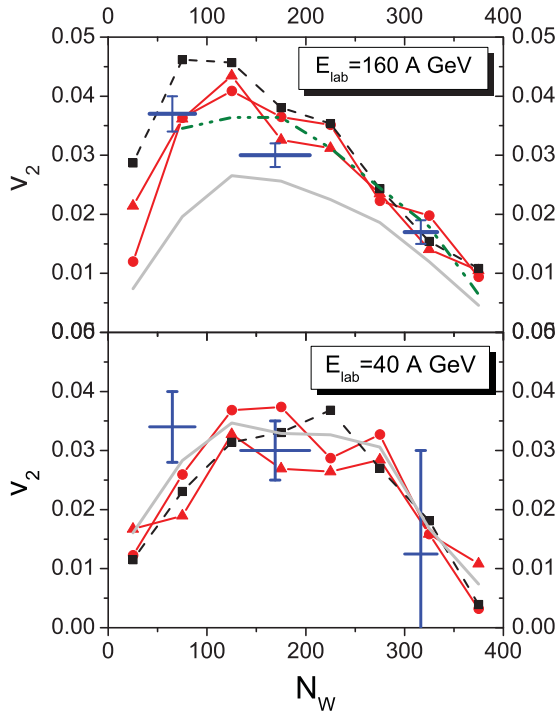


FIG. 11. (Color online) Centrality dependence of the charged particle elliptic flow at midrapidity $|y| < 0.5$ for collisions of Pb at beam energies of $E_{\text{lab}} = 40 \text{ A GeV}$ (lower plot) and 160 A GeV (upper plot). The line styles are as in the previous figure.

produced system can be regarded as being boost-invariant. To obtain a rapidity-independent density, we apply an additional cut in η , as described above, for the calculation of ρ_q . In this way, one effectively reduces the system to two dimensions and obtains a result that is comparable to that of the mere geometrical picture proposed in [63,75–78].

Figure 11 summarizes our results on the centrality dependence of the elliptic flow of charged pions, with $v_2 = \langle \cos[2(\phi - \Phi_R)] \rangle$, where Φ_R denotes the reaction plane. Again, both beam energies $E_{\text{lab}} = 40$ and 160 A GeV are depicted. A general challenge for the experimental determination of v_2 is the correct determination of the reaction plane, which sets the coordinate system in which the elliptic flow is defined. The experimental systematic uncertainty is reflected in large error bars and is especially severe at the lower energies. Nevertheless, our calculations show that the value of v_2 is hardly sensitive to the approach used for the calculations. All results, from the default UrQMD and the hybrid model, essentially give the same centrality dependence of v_2 at 40 A GeV . At the highest SPS beam energy, the picture is already different. Here the default UrQMD results underestimate the elliptic flow, while the default hybrid model overestimates it. Again, the core-corona separated version of the hybrid model improves the description.

VI. CONCLUSION

We presented a method to explore the dynamics of the system produced in high-energy heavy-ion collisions and to

effectively divide it into an equilibrated core and a dilute corona. Toward this end, the UrQMD hybrid approach was applied, in which the dense and equilibrated core is described hydrodynamically and the dilute corona is described by the nonequilibrium transport approach. To distinguish between the two separated regions, we employed a local particle density criterion.

It was found that the fraction of the system that can be regarded as being in local thermal and chemical equilibrium slowly increases in the energy range between $E_{\text{lab}} = 5$ and 40 A GeV . While observables of nonstrange hadrons appeared to be insensitive to this separation, strange hadron properties showed considerable modifications. Strange particle yields as well as their radial flow and especially the description of the “horn” in the K^+/π^+ ratio were improved. From this point of view, we explained the drastic increase in the K^+/π^+ up to $E_{\text{lab}} = 20\text{--}30 \text{ A GeV}$ with an onset of chemical equilibration of strangeness. In thermal models, which also explain the steep increase in strangeness production [95–98], canonical corrections or the introduction of a strangeness saturation parameter are usually responsible for the suppression of strangeness at low energies.

If the rapid equilibration of strangeness is caused by a change in the properties of the active degrees of freedom present in the initial state of the collision, then the present study suggests an onset of such a new phase in reactions at beam energies of $E_{\text{lab}} \approx 5\text{--}40 \text{ A GeV}$. In fact, the change of the properties of the matter involved would not change suddenly at some specific beam energy but rather continuously over a wide range of collision energies.

In the second part of this paper, we discussed the centrality dependence of different hadronic observables within the core-corona separated approach. Again, the description of strange hadron observables is improved in the core-corona version when compared to the default hybrid model. On the other hand, the hybrid model gives no good description of the excitation function of the mean transverse mass of pions and the centrality dependence of pion multiplicities, independent of the core-corona separation. For our model, we apply an ideal fluid dynamical description without viscous corrections. This is a possible origin for both observations, as viscosity leads to entropy production, which is directly related to the pion production rate. Furthermore, it can account for a decrease in the average flow in the hydrodynamic phase. Another contribution to the too small pion yield, as well as the too large average momentum, are missing contributions from high mass (mesonic) resonances, decaying predominantly into pions, which are not explicitly included in the Cooper-Frye transition and the transport model (as well as in the UrQMD model).

At the highest SPS energy, we only obtain a very moderate centrality dependence of the core fraction of the system. This is somewhat in contrast to studies in which the core fraction is calculated only on a two-dimensional projection of the system on the transverse plane, indicating that the system produced at $E_{\text{lab}} = 160 \text{ A GeV}$ seems to have a rapidity-independent density. As the Lorentz contraction of the incoming nuclei is also rather strong, a Lorentz-invariant formulation of the density as well as the hydrodynamic equations seems more

suitable. To approximate a rapidity-independent density, we applied a cut in η for the definition of the local particle density leading to a considerable improvement of the centrality dependence of strange particle yields, which supports a definition of the core as proposed in [63,75], at least at energies above $E_{\text{lab}} \approx 160A$ GeV. However, at lower energies, a full three-dimensional evaluation of the created system is in order.

ACKNOWLEDGMENTS

This work was supported by BMBF, HGS-hire, and the Hessian LOEWE Initiative through the Helmholtz International Center for FAIR (HIC for FAIR). The authors thank D. Rischke for providing the SHASTA code and Dr. H. Petersen for fruitful discussions. The computational resources were provided by the Frankfurt LOEWE Center for Scientific Computing (LOEWE-CSC).

-
- [1] M. Gyulassy and L. McLerran, *Nucl. Phys. A* **750**, 30 (2005).
 [2] C. Hohne (CBM Collaboration), *Nucl. Phys. A* **749**, 141 (2005).
 [3] J. Adams *et al.* (STAR Collaboration), *Nucl. Phys. A* **757**, 102 (2005).
 [4] B. B. Back *et al.*, *Nucl. Phys. A* **757**, 28 (2005).
 [5] I. Arsene *et al.* (BRAHMS Collaboration), *Nucl. Phys. A* **757**, 1 (2005).
 [6] K. Adcox *et al.* (PHENIX Collaboration), *Nucl. Phys. A* **757**, 184 (2005).
 [7] Z. Fodor, S. D. Katz, and K. K. Szabo, *Phys. Lett. B* **568**, 73 (2003).
 [8] C. R. Allton *et al.*, *Phys. Rev. D* **66**, 074507 (2002).
 [9] C. R. Allton, S. Ejiri, S. J. Hands, O. Kaczmarek, F. Karsch, E. Laermann, and C. Schmidt, *Phys. Rev. D* **68**, 014507 (2003).
 [10] C. R. Allton *et al.*, *Phys. Rev. D* **71**, 054508 (2005).
 [11] P. de Forcrand and O. Philipsen, *Nucl. Phys. B* **673**, 170 (2003).
 [12] E. Laermann and O. Philipsen, *Annu. Rev. Nucl. Part. Sci.* **53**, 163 (2003).
 [13] M. D'Elia and M. P. Lombardo, *Phys. Rev. D* **70**, 074509 (2004).
 [14] M. D'Elia and M. P. Lombardo, *Phys. Rev. D* **67**, 014505 (2003).
 [15] J. Y. Ollitrault, *Phys. Rev. D* **46**, 229 (1992).
 [16] D. H. Rischke, *Nucl. Phys. A* **610**, 88C (1996).
 [17] H. Sorge, *Phys. Rev. Lett.* **78**, 2309 (1997).
 [18] H. Heiselberg and A. M. Levy, *Phys. Rev. C* **59**, 2716 (1999).
 [19] S. Scherer *et al.*, *Prog. Part. Nucl. Phys.* **42**, 279 (1999).
 [20] S. Soff, S. A. Bass, M. Bleicher, H. Stoecker, and W. Greiner, [arXiv:nucl-th/9903061](https://arxiv.org/abs/nucl-th/9903061).
 [21] J. Brachmann *et al.*, *Phys. Rev. C* **61**, 024909 (2000).
 [22] L. P. Csernai and D. Rohrich, *Phys. Lett. B* **458**, 454 (1999).
 [23] B. Zhang, M. Gyulassy, and C. M. Ko, *Phys. Lett. B* **455**, 45 (1999).
 [24] P. F. Kolb, J. Sollfrank, and U. W. Heinz, *Phys. Rev. C* **62**, 054909 (2000).
 [25] M. Bleicher and H. Stöcker, *Phys. Lett. B* **526**, 309 (2002).
 [26] H. Stöcker, *Nucl. Phys. A* **750**, 121 (2005).
 [27] X. Zhu, M. Bleicher and H. Stöcker, *Phys. Rev. C* **72**, 064911 (2005).
 [28] H. Petersen, Q. Li, X. Zhu, and M. Bleicher, *Phys. Rev. C* **74**, 064908 (2006).
 [29] M. Gazdzicki *et al.* (NA49 Collaboration), *J. Phys. G* **30**, S701 (2004).
 [30] M. Gazdzicki and M. I. Gorenstein, *Acta Phys. Polon. B* **30**, 2705 (1999).
 [31] P. Koch, B. Muller, and J. Rafelski, *Phys. Rep.* **142**, 167 (1986).
 [32] E. L. Bratkovskaya, W. Cassing, C. Greiner, M. Effenberger, U. Mosel, and A. Sibirtsev, *Nucl. Phys. A* **681**, 84 (2001).
 [33] P. Braun-Munzinger, J. Stachel, and C. Wetterich, *Phys. Lett. B* **596**, 61 (2004).
 [34] C. Greiner, P. Koch-Steinheimer, F. M. Liu, I. A. Shovkovy, and H. Stoecker, *J. Phys. G* **31**, S725 (2005).
 [35] J. Hofmann, H. Stöcker, U. W. Heinz, W. Scheid, and W. Greiner, *Phys. Rev. Lett.* **36**, 88 (1976).
 [36] H. Stöcker and W. Greiner, *Phys. Rep.* **137**, 277 (1986).
 [37] C. M. Hung and E. V. Shuryak, *Phys. Rev. Lett.* **75**, 4003 (1995).
 [38] D. H. Rischke, S. Bernard, and J. A. Maruhn, *Nucl. Phys. A* **595**, 346 (1995).
 [39] C. E. Aguiar, T. Kodama, T. Osada, and Y. Hama, *J. Phys. G* **27**, 75 (2001).
 [40] P. F. Kolb and U. W. Heinz, [arXiv:nucl-th/0305084](https://arxiv.org/abs/nucl-th/0305084).
 [41] R. Baier and P. Romatschke, *Eur. Phys. J. C* **51**, 677 (2007).
 [42] H. Song and U. W. Heinz, *Phys. Rev. C* **77**, 064901 (2008).
 [43] B. Schenke, S. Jeon, and C. Gale, *Phys. Rev. C* **82**, 014903 (2010).
 [44] K. Werner, I. Karpenko, T. Pierog, M. Bleicher, and K. Mikhailov, *Phys. Rev. C* **82**, 044904 (2010).
 [45] D. Molnar and P. Huovinen, *Phys. Rev. Lett.* **94**, 012302 (2005).
 [46] Z. Xu and C. Greiner, *Phys. Rev. C* **71**, 064901 (2005).
 [47] G. Baur, J. Bleibel, C. Fuchs, A. Faessler, L. V. Bravina, and E. E. Zabrodin, *Phys. Rev. C* **71**, 054905 (2005).
 [48] S. A. Bass *et al.*, *Prog. Part. Nucl. Phys.* **41**, 255 (1998).
 [49] M. Bleicher *et al.*, *J. Phys. G* **25**, 1859 (1999).
 [50] W. Cassing and E. L. Bratkovskaya, *Phys. Rev. C* **78**, 034919 (2008).
 [51] O. Linnyk, E. L. Bratkovskaya, and W. Cassing, *J. Phys. G* **37**, 094039 (2010).
 [52] V. K. Magas, L. P. Csernai, and D. Strottman, [arXiv:hep-ph/0110347](https://arxiv.org/abs/hep-ph/0110347).
 [53] H. Song, S. A. Bass, and U. Heinz, *Phys. Rev. C* **83**, 054912 (2011).
 [54] S. Paiva, Y. Hama, and T. Kodama, *Phys. Rev. C* **55**, 1455 (1997).
 [55] C. E. Aguiar, Y. Hama, T. Kodama, and T. Osada, *Nucl. Phys. A* **698**, 639 (2002).
 [56] D. Teaney, J. Lauret, and E. V. Shuryak, [arXiv:nucl-th/0110037](https://arxiv.org/abs/nucl-th/0110037).
 [57] O. J. Socolowski, F. Grassi, Y. Hama, and T. Kodama, *Phys. Rev. Lett.* **93**, 182301 (2004).
 [58] T. Hirano, U. W. Heinz, D. Kharzeev, R. Lacey, and Y. Nara, *Phys. Lett. B* **636**, 299 (2006).
 [59] T. Hirano, U. W. Heinz, D. Kharzeev, R. Lacey, and Y. Nara, *Phys. Rev. C* **77**, 044909 (2008).
 [60] S. A. Bass, A. Dumitru, M. Bleicher, L. Bravina, E. Zabrodin, H. Stöcker, and W. Greiner, *Phys. Rev. C* **60**, 021902 (1999).
 [61] C. Nonaka and S. A. Bass, *Phys. Rev. C* **75**, 014902 (2007).
 [62] A. Dumitru, S. A. Bass, M. Bleicher, H. Stoecker, and W. Greiner, *Phys. Lett. B* **460**, 411 (1999).
 [63] K. Werner, *Phys. Rev. Lett.* **98**, 152301 (2007).
 [64] F. Becattini and J. Manninen, *J. Phys. G* **35**, 104013 (2008).
 [65] H. Petersen, M. Bleicher, S. A. Bass, and H. Stöcker, [arXiv:hep-ph/0805.0567](https://arxiv.org/abs/hep-ph/0805.0567).
 [66] A. Rebhan, P. Romatschke, and M. Strickland, *Phys. Rev. Lett.* **94**, 102303 (2005).

- [67] C. Nonaka and S. A. Bass, *Nucl. Phys. A* **774**, 873 (2006).
- [68] T. Hirano and M. Gyulassy, *Nucl. Phys. A* **769**, 71 (2006).
- [69] H. Petersen, J. Steinheimer, G. Burau, M. Bleicher, and H. Stöcker, *Phys. Rev. C* **78**, 044901 (2008).
- [70] J. Steinheimer, M. Bleicher, H. Petersen, S. Schramm, H. Stöcker, and D. Zschesche, *Phys. Rev. C* **77**, 034901 (2008).
- [71] J. Steinheimer, M. Mitrovski, T. Schuster, H. Petersen, M. Bleicher, and H. Stoecker, *Phys. Lett. B* **676**, 126 (2009).
- [72] J. Steinheimer, S. Schramm, and H. Stöcker, *J. Phys. G* **38**, 035001 (2011).
- [73] F. Cooper and G. Frye, *Phys. Rev. D* **10**, 186 (1974).
- [74] J. Steinheimer, V. Dexheimer, M. Bleicher, H. Petersen, S. Schramm, and H. Stöcker, *Phys. Rev. C* **81**, 044913 (2010).
- [75] J. Aichelin and K. Werner, *Phys. Rev. C* **79**, 064907 (2009).
- [76] F. Becattini and J. Manninen, *Phys. Lett. B* **673**, 19 (2009).
- [77] J. Aichelin and K. Werner, *J. Phys. G* **37**, 094006 (2010).
- [78] J. Aichelin and K. Werner, *Phys. Rev. C* **82**, 034906 (2010).
- [79] C. Alt *et al.* (NA49 Collaboration), *Phys. Rev. C* **78**, 034918 (2008).
- [80] S. V. Afanasiev *et al.* (The NA49 Collaboration), *Phys. Rev. C* **66**, 054902 (2002).
- [81] L. Ahle *et al.* (E866 Collaboration and E917 Collaboration), *Phys. Lett. B* **476**, 1 (2000).
- [82] J. Adams *et al.* (STAR Collaboration), *Phys. Rev. Lett.* **92**, 112301 (2004).
- [83] K. Adcox *et al.* (PHENIX Collaboration), *Phys. Rev. C* **69**, 024904 (2004).
- [84] J. L. Klay *et al.* (E-0895 Collaboration), *Phys. Rev. C* **68**, 054905 (2003).
- [85] C. Alt *et al.* (NA49 Collaboration), *Phys. Rev. C* **77**, 024903 (2008).
- [86] M. K. Mitrovski *et al.* (NA49 Collaboration), *J. Phys. G* **32**, S43 (2006).
- [87] H. Petersen, J. Steinheimer, M. Bleicher, and H. Stöcker, *J. Phys. G* **36**, 055104 (2009).
- [88] A. Bialas, M. Bleszynski, and W. Czyz, *Nucl. Phys. B* **111**, 461 (1976).
- [89] K. J. Eskola, K. Kajantie, and J. Lindfors, *Nucl. Phys. B* **323**, 37 (1989).
- [90] T. Anticic *et al.* (NA49 Collaboration), *Phys. Rev. C* **80**, 034906 (2009).
- [91] C. Alt *et al.* (NA49 Collaboration), *Phys. Rev. Lett.* **94**, 052301 (2005).
- [92] C. Alt *et al.* (NA49 Collaboration), *Phys. Rev. Lett.* **94**, 192301 (2005).
- [93] C. Alt *et al.* (NA49 Collaboration), *Phys. Rev. C* **68**, 034903 (2003).
- [94] H. Petersen, M. Mitrovski, T. Schuster, and M. Bleicher, *Phys. Rev. C* **80**, 054910 (2009).
- [95] A. Andronic, P. Braun-Munzinger, and J. Stachel, *Nucl. Phys. A* **772**, 167 (2006).
- [96] A. Andronic, P. Braun-Munzinger, and J. Stachel, *Phys. Lett. B* **673**, 142 (2009).
- [97] F. Becattini, M. Gazdzicki, A. Keranen, J. Manninen, and R. Stock, *Phys. Rev. C* **69**, 024905 (2004).
- [98] F. Becattini, J. Cleymans, A. Keranen, E. Suhonen, and K. Redlich, *Phys. Rev. C* **64**, 024901 (2001).